Influence of calcium to silica ratio on H_2 gas production in calcium silicate hydrate

C. Yin, A. Dannoux-Papin, J. Haas, Jean-Philippe Renault

Influence of calcium to silica ratio on H_2 gas production in calcium silicate hydrate

YIN C.[1], DANNOUX-PAPIN A.[1], HAAS J.[1], RENAULT J-P.[2]

[1]CEA, DEN, MAR, DE2D, SEAD, Laboratoire d'études des Ciments et Bitumes pour le Conditionnement, F-30207 Bagnols sur Cèze Cedex, France

[2]CEA, DRF, IRAMIS, NIMBE, Laboratoire Interdisciplinaire sur l'Organisation Nanométrique et Supramoléculaire, 91191 Gif-sur-Yvette Cedex, France

HIGHLIGHTS

- Efficient hydrogen production from irradiated calcium silicate hydrate
- Ca^{2+} ions do not promote more efficiently H_2 formation
- Efficient energy transfers from calcium silicate hydrate to water
- Mechanisms of water radiolysis in calcium silicate hydrate is proposed

ABSTRACT

Water radiolysis is of particular concern for the conditioning of radioactive waste with cement materials. For safety assessment, water radiolysis issued from pore solution and hydrates must be considered because radiolytic molecular hydrogen H_2 is produced, which is potentially explosive. Calcium silicate hydrate (C-S-H), main hydrates with Portlandite in Portland cements, were synthesised with different C/S ratios at 60% relative humidity. The samples were characterized by X-ray diffraction and thermogravimetric analysis before irradiation. Then, samples were irradiated under γ-irradiation,

and the radiolytic hydrogen production has been quantified. The results show that, in these conditions, the H_2 production in CSH is comparable to the one in bulk water, with primary yield ranging from 0.35 to 0.6 molecule/100eV.

1. INTRODUCTION

In France, some of low and intermediate level wastes issued from the dismantling of nuclear facilities are conditioned in calcium silicate cements to ensure the stability and the confinement of the radioactivity for disposal and future geological storage. From an industrial point of view, cement-based materials are good candidates to store large quantities of nuclear waste as they are inexpensive, easy to produce and can be tailored to reach various different properties such as soundness, strength. However, when cements are submitted to ionizing radiation, hydrogen gas is released and its potential reactivity has drawn great attention for the safety of nuclear waste disposal [1]. In order to not exceed the lower flammability limit (LFL) [1], the hydrogen release from the cementitious packages must be limited and quantified. Since it is a material with various possible compositions and a complex nano- and micro- structure [2], [3], the radiolytic process leading to hydrogen release in such material is challenging and not well understood.

The behaviour of cement paste [4], [5], [6], [7], [8] under irradiation is well described in the literature in terms of the radiolysis of pore water and therefore the radiolytic hydrogen emission. Their stability under irradiation up to several GGy of absorbed doses makes choice materials for packaging waste. In addition, a decrease in mechanical strength is explained by the decomposition of hydrates, the

appearance of amorphous phases and the dissociation of chemically bound water [9]. However, the mechanism of H_2 production is not completely understood and recent studies [9], [10] have shown that, beside the pore water, the water of hydration ("bound") of different hydrates contributes as well to the radiolytic hydrogen production.

In such hydrated compounds, radiolysis is not well described and the literature is quite limited. In minerals, ionizing irradiation induces electronic defects that promote H° radicals and oxygen center holes. The H° radicals should be trapped in the structure, recombine with oxygen center holes or recombine with each other to form dihydrogen gas H_2. The probability of each process depends on the crystal structure, the acidity, the mobility and the content of hydroxide groups, the nature and the content of charge compensative cations and the amount of crystallization water.

In other porous structures such as, aluminum hydroxides [9], zeolite [11], controlled-pore glasses [12], geopolymer [13], and clays [14], [15], [16], [17], the water radiolysis has been already carefully studied using gamma-rays. In clays, water radiolysis studies showed strong modifications of the mechanisms involved with respect to bulk water because of confinement and interfacial phenomena that conducted to dramatic effects on reaction rates and radiolytic mechanisms [18], [19], [20], [21].

Moreover, few knowledge remains on the radiolysis of the water at the interface of hydrates and how it contributes to the stability of the cementitious material under irradiation. According to some authors [22], [23], [24], [25], [16], some specific effects should be expected in these materials such as energy transfers or diffusion of transient radiolytic species in solid and/or at the water/solid interface. C-S-H, which is the main product of the hydration of Portland cement, in radiolytic hydrogen release, needed obviously to be payed attention to.

According to Jennings [26], [27], the crystal chemistry of C-S-H should be modelled taking into account the “Feldman-Sereda” and “Power and Brownyard” hypothesis.

Structural relations among tobermorites and C-S-H have been studied by many workers [28]. The C-S-H are amorphous and layered structures that could be compared to the tobermorite [29]. In tobermorite, each sheet is composed of silicate chains that are connected with each other by calcium atoms as demonstrated by ^{29}Si MAS NMR measurements (**Figure** 1) [30], [31]. In tobermorite, two oxygens from non-bridging tetrahedral coordinate to calcium ions [28c], [32].

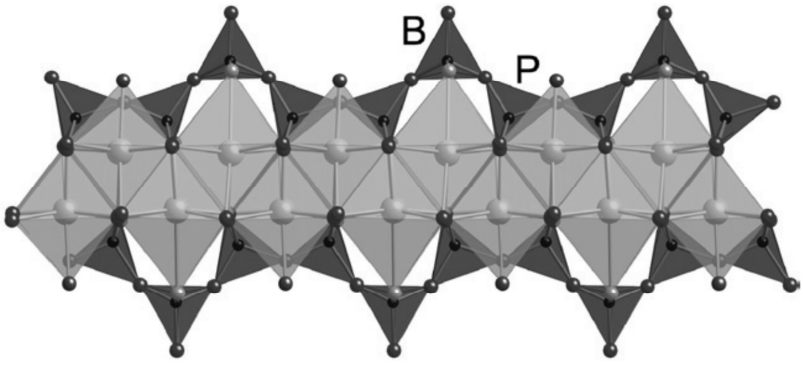

Figure 1. Single layer of 1.4-nm tobermorite illustrating dreierketten chains. The chains have a kinked pattern where some silicate tetrahedra share O−O edges with the central Ca−O layer (called ‘paired’ tetrahedra (P)), and others that do not (called ‘bridging’ tetrahedra (B)) [14].

In C-S-H, crystallization water is located in an interlayer space. The interlayer space varies with the C/S ratio and the interlayer distance increase from 9 to 14 Å [33], [34]. Consequently, water molecules are placed in a confined environment where the radiolysis of water can be strongly affected.

However, one must also consider that the layers associate to form grains of few nm.

A last radiolysable type of water is the chemically bound one, present as the form of hydroxide.

The purpose of the present work is to understand the water radiolysis in the C-S-H and how the solid/water interface can modify the radiolytic mechanisms: different C-S-H with varying C/S ratio (from 0.8 to 1.6) at controlled relative humidity of 60% are submitted to gamma irradiation.

2. MATERIALS AND METHODS

2.1 Synthesis of C-S-H

C-S-H samples were synthesized from pozzolanic reaction of amorphous silica (SiO_2, AEROSIL 380, Degussa) and CaO in excess of water. Reagent grade calcium carbonate ($CaCO_3$, VWR Company) was calcined at 960 °C for 24 hours to obtain calcium oxide, then it is stored in vacuum desiccator. Stoichiometric amounts of CaO and SiO_2 were mixed in order to produce C-S-H samples having C/S ratio of 0.8, 1.0, 1.2, 1.4 and 1.6. The materials were mixed with ultrapure water (Milli-Q 18 MΩ) at a water / solid mass ratio of 50 in 1 L high-density polyethylene (HDPE) bottles. The bottles were shaken on a rotating rack for 1 month. The synthesis was conducted at room temperature (i.e., 25°C). Once the desired time was reached, the remaining calcium and silicon ions concentrations in the solution were determined by ICP-AES.

Samples were filtered using a Büchner funnel and a filter paper (0.22 µm, Millipore) and rinsed with water and freeze-dried for 4 days. It should be noted that the use of organic solvent (isopropanol) to stop the hydration is not applied because of its potential contribution to radiolytic hydrogen production. Then, the samples were cured in desiccator chamber with 60% relative humidity under a nitrogen

atmosphere at room temperature for 4 weeks until their weight stabilized. The relative humidity was controlled by a sodium bromide saturated salt (ca. 60% RH).

2.2 Sample Characterization

2.2.1 X-Ray Diffraction

To check the purity of C-S-H samples, X-Ray diffraction experiments were performed on a Panalytical X'Pert Pro diffractometer (Bruker) with an RX tube using a copper anticathode (λKα1 = 1.54056 Å). The diffractometer was operated at 45 kV and 40mA. Measurements were made at a 2θ range from 5° to 70° with steps of 0.017° and a measurement time equivalent to 80 seconds per step. The detector is an Xcelerator (linear detector with120 points aligned detectors). The diffraction patterns were analysed using the Eva 21.0 software (Bruker).

2.2.2 Thermogravimetry analysis

Thermogravimetric analysis was performed to describe the dehydration process of C-S-H using a STA 409 PC Luxx® (Netzsch) from 25°C to 1000°C at a heating rate of 10 °C/min, with two hours at 300°C and two hours at 500°C. The analysis is conducted under nitrogen flux at 50 ml/min. Alumina crucibles were used and the sample weight was approximately 50 mg. Data were processed using Proteus Thermal Analysis (Netzsch). The derivative theromogravimetric (DTG) curve permits to determine the different loss of weight over the range of temperature. Acquisitions were performed on freeze-dried samples, equilibrated at 60% of relative humidity.

Table 2. Chemical composition in weight percentages calculated from thermogravimetry analysis of different C/S ratio samples cured at 60% RH.

Initial C/S ratio	Final C/S ratio	Water content	$Ca(OH)_2$ content	$CaCO_3$ content
0.8	0.80	18.9%	6.5%	3.2%
1.0	0.97	18.7%	4.2%	3.3%
1.2	1.14	17.2%	12.4%	4.0%
1.4	1.30	17.2%	8.6%	2.4%
1.6	1.40	16.9%	11.8%	5.6%

2.2.3 Nitrogen gas adsorption and desorption

Nitrogen gas adsorption-desorption cycles at 77K were determined using a Micromeritics ASAP 2020 surface area and porosity analyser. Samples were initially outgassed by using 0.3 g of each material under vacuum at 100 °C for 48 h to obtain the dry sample before analysis.

The specific surface area data were obtained using Brunauer-Emmett-Teller (BET) between 0.1 and 0.3 of relative pressure P/P0.

2.3 IRRADIATION EXPERIMENTS AND GAS ANALYSIS

C-S-H samples were γ-irradiated using a ^{60}Co source experimental irradiator at Marcoule (Gammatec, Steris, France). Approximately 120 mg were introduced in 12 mL Pyrex glass ampules, which were then flame-sealed under argon at about 900 mbar to avoid oxygen presence. Attention has been paid to not modify the water content of the samples during the sealing which has been confirmed by TGA measurements. Glass ampules were placed on a rotating plate to ensure the dose delivery spatial homogeneity. Dosimetry was performed with red Perspex dosimeters and the absorbed dose is known with a 5.6 % standard deviation. Samples were irradiated by

using an average dose rate of 600 Gy/h at 25 ± 1°C up to 100 and 200 kGy of absorbed doses. For each absorbed dose, two independent samples were irradiation.

The amount of dihydrogen produced during γ-irradiation was evaluated by using a micro-gas chromatography (490 Micro-GC, Agilent) equipped with a compression system (SRA Instruments) to provide 1 bar of pressure at the input of the μ-GC injector. The channel used for hydrogen analysis contains a Molecular Sieve 5A PLOT column under argon at 28 psi pressure and a micro thermal conductivity detector (μ-TCD). The oven and detector temperatures were respectively 90 and 120 °C, with an acquisition time of 2 minutes.

The hydrogen production yield, denoted as the G-value and expressed in mol/J, corresponds to the amount of dihydrogen produced per amount of absorbed energy. For each C-S-H sample, apparent hydrogen radiolytic yields $G(H_2)$ have been assessed by calculating the slope of the hydrogen production as a function of the absorbed dose. Normalized apparent hydrogen radiolytic yields $G_{norm}(H_2)$, expressed in mol/J, were calculated by normalizing apparent hydrogen radiolytic yields by the experimentally measured initial water mass fraction. Yields standard deviations are estimated to be less than 10 %.

3. RESULTS

3.1 Sample chemical composition

The experimental C/S ratios were indirectly checked by chemical analysis of the solution at the end of the synthesis (**Table** 1), the amount of portlandite and calcite is neglected in the calculation.

pH values and [CaO], [SiO_2] in solution according to C/S ratio indicate that samples are in the equilibrium according to the solubility curve according to the literature.

Table 1. Real compositions of the synthesized phases.

[CaO] (mmol/L)	151.7	167.4	179.87	188.3	187.3
[SiO_2] (mmol/L)	190.3	172.4	157.19	144.5	133.7
Experimental C/S ratio	0.80	0.97	1.14	1.30	1.40
pH value of the solution	11.3	12.1	12.2	12.5	12.5

3.1 X-Ray powder Diffraction

The purity of C-S-H samples was controlled by X-Ray powder Diffraction (XRD). The experimental patterns show that all the samples present the diffraction peaks corresponding to the tobermorite structure [35] (**Figure** 2). For nominal C/S ratio from 0.80, to 1.14, the diffractograms do not reveal other peaks. Then, the pozzolanic reaction is complete and the C-S-H are considered pure. It is noticed that, for samples with C/S ratio at 1.30 and 1.40, additional peaks appear that are attributed to a small amount of portlandite and calcite. The presence of portlandite and calcite is quantified by TGA analysis in Table 2.

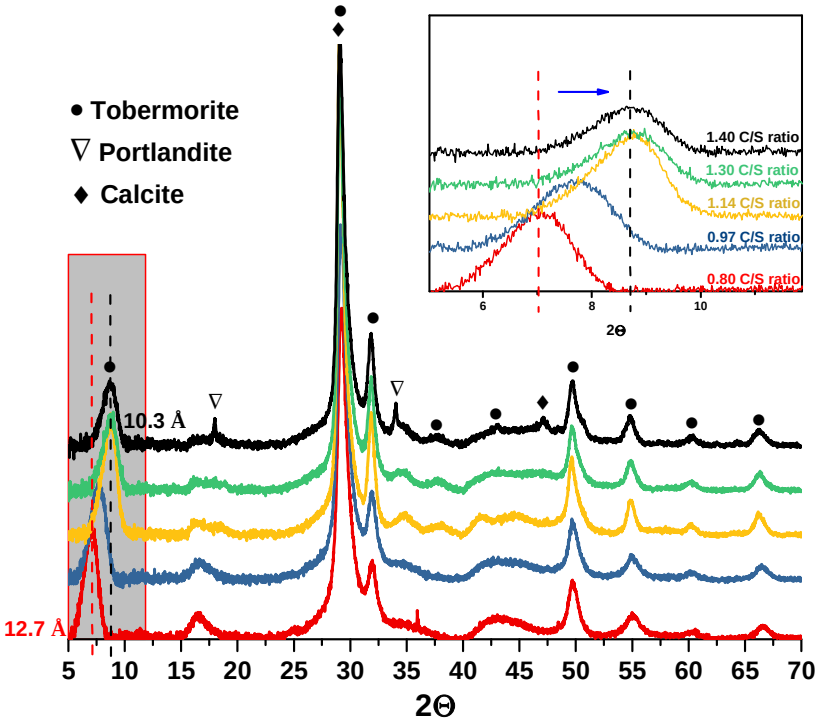

Figure 2. Powder XRD patterns of the different C-S-H samples (From bottom to top: 0.80, 0.97, 1.14, 1.30 and 1.40 CSH RH=60%).

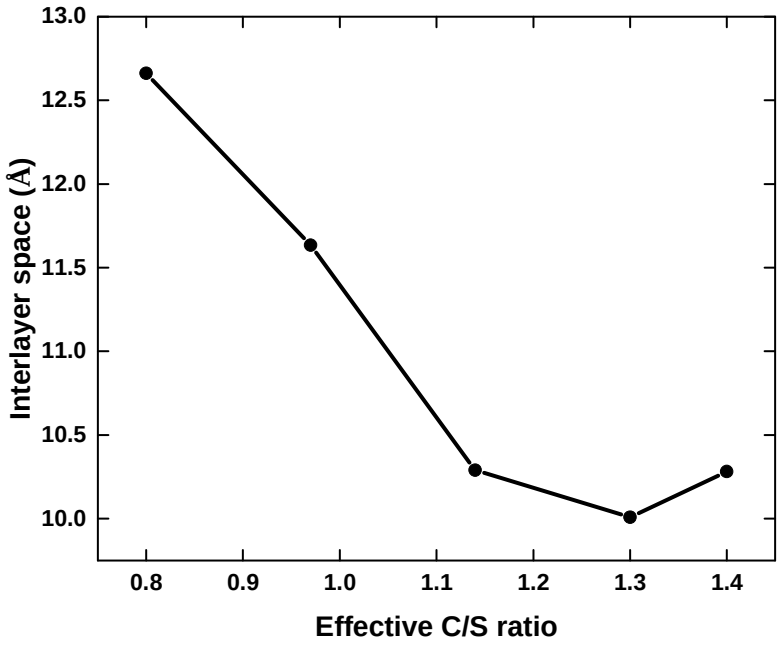

Figure 3. Interlayer space as a function of the C/S ratio at 60% RH.

The main differences between the various C-S-H XRD patterns with different C/S ratio acquired at 60% RH are the position and the intensity of the peak at 7.2−9.1° and 30° (2θ). The position of the first peak corresponds to the (001) reflection and reveals the interlayer distance using the structural model described by Grangeon et al [35]. At C/S ratio of 1.40, 1.30, 1.14, 0.97 and 0.80 ratio, the (001) reflection evolves from 10.0 to 12.7 Å that is in good agreement with previous study [33]. (**Figure** 3) Noticingly, the interlayer distance vary very little between C/S of 1.1 and 1.4

3.2 Thermogravimetry analysis

Table 2 summarized the results of TGA and the thermograms were shown in Figure 4.

All the TGA analyses showed extremely similar curves. Two steps of decomposition are observed. The first one (from 30 to 300°C) corresponds to the loss of the sum of pore water, crystallization water and hydroxides. We must notice that the amount of water trapped into the material vary less than the corresponding interlayer distance (the amount of water decreases by 10% table 1, when the distance decreases by 30%)

The second step (from 300 to 500°C) corresponds to the decomposition of few amounts of portlandite ($Ca(OH)_2$). In the third step, the weight loss (from 500 to 750°C) results from the decomposition of carbonates. Note that temperature boundaries are approximate and depend on the heating rate and on how the water interacts with solid surfaces. Hydration state is determined by thermogravimetry analysis in order to quantify the water and the portlandite amounts and to detect the eventual carbonation. The appearance of portlandite is probably due to the further hydration process during the storage. Such results can be interpreted by the

fact that the organic solvent is not applied in our protocol. The formation of carbonation could be due to the well-known reason of the existence of the atmospheric CO_2. The rate of carbonation of C-S-H is increasing with the pH.

As a consequence, the amount of portlandite and carbonate increase with increasing C/S ratio, which is the common observation in the previous literature.

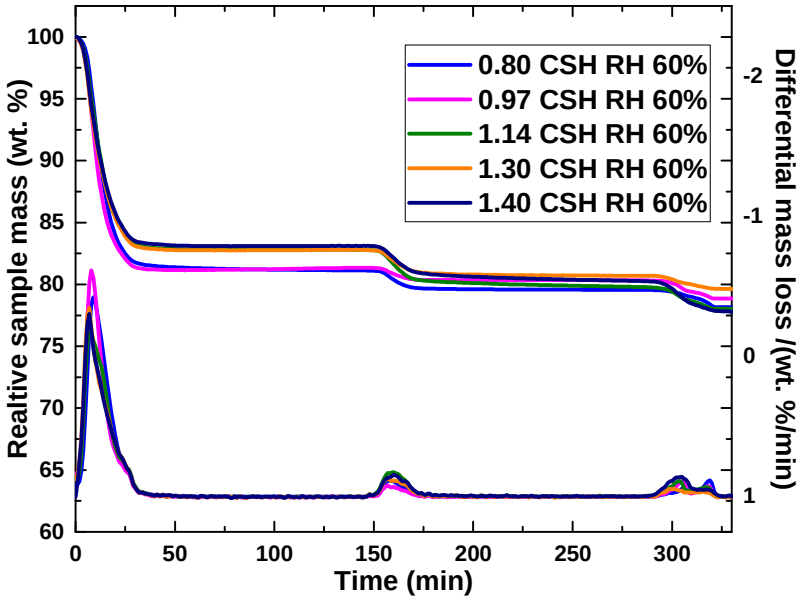

Figure 4. TG and DTG curves of 0.80, 0.97, 1.14, 1.30 and 1.40 C/S ratio CSH samples at RH 60%. DTG curves are given to illustrate the water loss and the detection of minor phases such as portlandite and calcium carbonate.

3.3 Nitrogen adsorption/desorption

From the different C-S-H samples, the isotherms were all type-IV according to IUPAC, which is characteristic of a mesoporous material. The H3-type hysteresis loop is linked with the non-rigid nature of the adsorbent and the location of the characteristic shoulder ($0.42P_0$) is consistent with the destabilization of condensate at the limiting P/P0 value. The type H3 hysteresis loops are typically

given by the adsorption of nonpolar gases by montmorillonite clays [36],[37] and the aggregates of other platy particles.

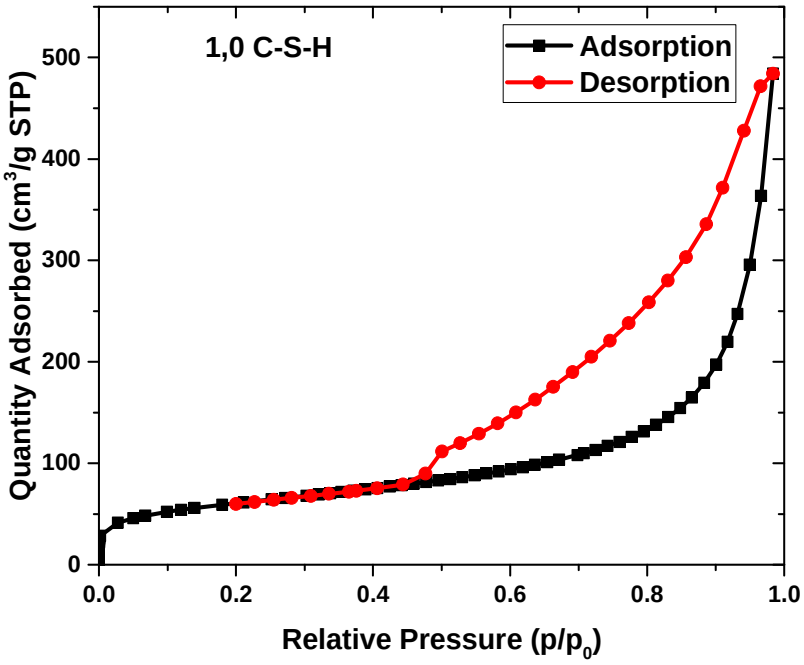

Figure 5. Nitrogen adsorption/desorption isotherms of 1.0 C/S ratio CSH sample.

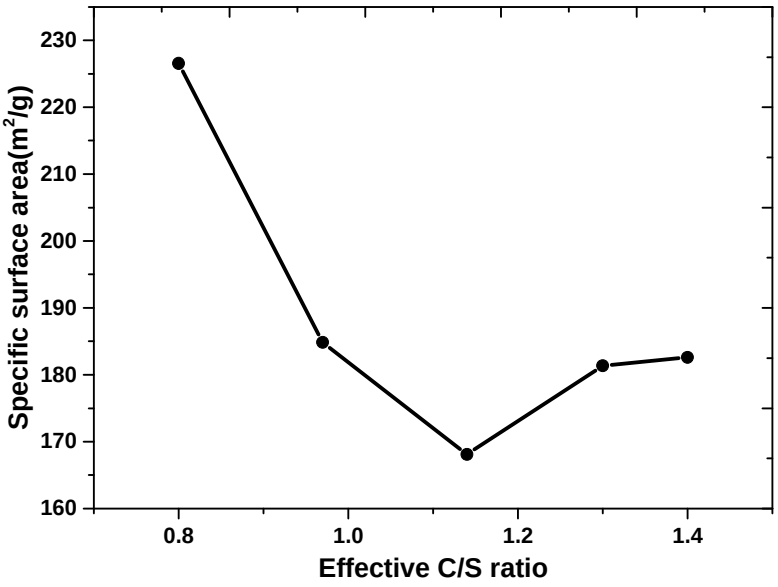

Figure 6. The specific surface area as a function of the effective C/S ratio.

At C/S ratio 0.8, C-S-H has the highest specific surface area which is 226 m^2/g. Then, with increasing C/S ratio from 0.80 to 1.14, the specific surface area decreases. This could be explained by an increase of the grain size from C-S-H 0.8 to C-S-H 1.2, which has

been interpreted by Roosz [38], as an increase of the number of layers stacked along c axis. At higher ratios, C-S-H 1.6 displays a higher value (183 m^2/g) than C-S-H 1.2. This could be due to the precipitation of portlandite nanoparticles and detected by TGA and XRD, during the drying step, which tends to increase the surface area of the C-S-H 1.6. according to a platelike morphology [38].

3.4 Hydrogen production under gamma irradiation

Table 3. Hydrogen radiolytic yields released from Gamma irradiated samples hydrated at 60% at room temperature.

Effective C/S ratio	$G(H_2)$ (mol/J×10^{-7}) (calculated with respect to the total energy received by the system)	$G(H_2)$ (mol/J×10^{-7}) (calculated with respect to the energy received solely by water)
0.80	0.61±0.06	3.23±0.32
0.97	0.58±0.06	3.11±0.31
1.14	0.49±0.05	2.85±0.29
1.30	0.42±0.04	2.44±0.24
1.40	0.36±0.04	2.13±0.21

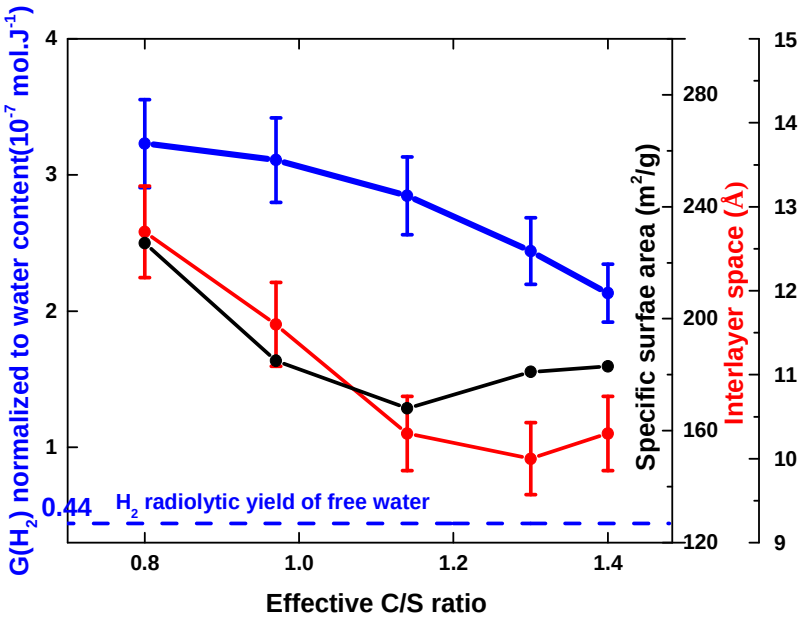

Figure 7. The normalized H_2 radiolytic yields (in blue colour), the specific surface area (in black colour) and the interlayer distance (in red colour) as a function of the

experimental C/S ratio. The value obtained in liquid bulk water is given as a comparison (4.4×10^{-8} mol J^{-1}) to reveal the specific behaviour of confined water.

When hydrates were exposed to gamma radiation, the H_2 gas was produced. Radiolytic yields were presented in **Table** 3. It is shown from the figure that radiolytic hydrogen production decreases with increasing C/S ratio from 0.8 to 1.4 (**Figure** 7), the radiolytic hydrogen production from portlandite and calcite could be neglected under gamma irradiation comparing to C-S-H because their effects are under uncertainty.

As reference, the molecular yield of dihydrogen obtained under γ-irradiation of bulk aqueous solutions, in the presence of 10^{-3} M bromide to protect the molecular hydrogen from OH radical attack, is 4.4×10^{-8} mol J^{-1} [39], [40].

The first results show that all the values of $G_{norm}(H_2)$ in C-S-H (that is in the absence of any radical scavenger) are approximately 3 to 6 times higher than $G(H_2)$ in bulk water. These yields are important and show that the radiolytic phenomena that occur in water confined in C-S-H are different to those in bulk water. But they are not exceptionally important and remain compatible either with a scavenging/ trapping of the oxidative species [9] leading to a preferential recombination of reductive species (1-3) and/ or to an efficient energy transfer from the material to the neighbouring OH groups (4-6).

$$H^\circ + H^\circ \rightarrow H_2 \quad (1)$$

$$e^-_{aq} + e^-_{aq} \rightarrow H_2 + 2OH^- \quad (2)$$

$$e^-_{aq} + H^\circ \rightarrow H_2 + OH^- \quad (3)$$

Indeed, energy transfers in hydroxide systems are usually associated with electron migration from the material towards surface OH groups

$$CSH \xrightarrow{\gamma} e^- + h^+ \quad (4)$$

$$e^- + ROH \rightarrow RO^- + H^\circ \quad (5)$$

$$H^\circ + H^\circ \rightarrow H_2 \quad (6)$$

The second result is the decrease of the yields when the ratio C/S increases.

In clays, the interlayer distance was a major parameter in controlling the H_2 production [16] , with a non monotoneous $G(H_2)$ evolution with this distance.

The problem in the interpretation of our result is that three types of water must be considered here [38].

-the interlayer water

-the external water, adsorbed as a multilayer at the considered RH

-the surface hydroxyl groups

The amount of external water and the grain size decreases when C/S increases, whereas the amount of interlayer water and hydroxyl groups are thought to increase [38].

This obviously suggests that the radiolyzable sites (ROH in equation 5) are located on the surface of the grains. Indeed, the Figure 7 show that the specific surface and the $G(H_2)$ are well connected., Studies at different relative humidities will be probably necessary to confirm this fact.

However, the variation of C/S change also the nature of the material itself, with Ca^{2+} ions increasing, changes in electronic densities or in bridging and non-bridging oxygens.

Sophie Le Caer et al. [4] studied cement paste and point out that the water-rich interlayer regions with Ca^{2+} ions act as electrons traps that promote the formation of H_2. But we don't have any evidence in our case that C-S-H hydrates richer in Ca^{2+} ions promote more efficiently H_2 formation.

The fate of the oxidative species (the hole in reaction 4) remain largely unknown in CSH. However, as no oxygen production was measured here, they remain probably trapped as accumulating defects within the material. To further understand this part of CSH radiolysis, radiation induced transient species in C-S-H should be probed by Electron Spin Resonance spectroscopy (ESR).

4. CONCLUSIONS

The production of radiolytic dihydrogen different C-S-H samples submitted to y-irradiation has been quantified. First results confirm an enhancement of hydrogen production in C-S-H hydrates compared to that in bulk water and an evolution of hydrogen production with varying the effective C/S ratio. Indeed, the greater specific surface of low C/S ratio involves a greater hydrogen release. But the radiolytic mechanisms involved require more studies and the influence of various parameters such as porosity, water content, and secondary minor phases should be investigated.

4. REFERENCES

[1] B. Bonin, M. Colin, A. Dutfoy, *Journal of Nuclear Materials* **2000**, *281*, 1-14.

[2] R. J.-M. Pellenq, A. Kushima, R. Shahsavari, K. J. Van Vliet, M. J. Buehler, S. Yip, F.-J. Ulm, *Proceedings of the National Academy of Sciences* **2009**, *106*, 16102-16107.

[3] A. J. Allen, J. J. Thomas, H. M. Jennings, *Nature materials* **2007**, *6*, 311-316.

[4] S. Le Caër, L. Dezerald, K. Boukari, M. Lainé, S. Taupin, R. M. Kavanagh, C. S. N. Johnston, E. Foy, T. Charpentier, K. J. Krakowiak, R. J. M. Pellenq, F. J. Ulm, G. A. Tribello, J. Kohanoff, A. Saúl, *Cement and Concrete Research* **2017**, *100*, 110-118.

[5] R. C. Ewing, W. J. Weber, F. W. Clinard, *Progress in Nuclear Energy* **1995**, *29*, 63-127.

[6] L. Dezerald, J. J. Kohanoff, A. A. Correa, A. Caro, R. J. M. Pellenq, F. J. Ulm, A. Saúl, *Environmental Science & Technology* **2015**, *49*, 13676-13683.
[7] P. Bouniol, E. Bjergbakke, *Journal of Nuclear Materials* **2008**, *372*, 1-15.
[8] P. Bouniol, B. Muzeau, V. Dauvois, *Journal of Nuclear Materials* **2013**, *437*, 208-215.
[9] J. A. Kaddissy, S. Esnouf, D. Durand, D. Saffre, E. Foy, J.-P. Renault, *The Journal of Physical Chemistry C* **2017**, *121*, 6365-6373.
[10] D. Chartier, J. Sanchez-Canet, B. Laetitia, S. Esnouf, J. P. Renault, *Influence of formulation parameters of cement based materials towards gas production under gamma irradiation, Vol. 511*, **2018**.
[11] L. Frances, M. Grivet, J.-P. Renault, J.-E. Groetz, D. Ducret, *Radiation Physics and Chemistry* **2015**, *110*, 6-11.
[12] S. Le Caër, P. Rotureau, F. Brunet, T. Charpentier, G. Blain, J. P. Renault, J. C. Mialocq, *ChemPhysChem* **2005**, *6*, 2585-2596.
[13] F. Chupin, A. Dannoux-Papin, Y. N. Ravache, J.-B. d. E. de Lacaillerie, *Journal of Nuclear Materials* **2017**, *494*, 138-146.
[14] J. K. Thomas, *Chemical reviews* **1993**, *93*, 301-320.
[15] C. Fourdrin, H. Aarrachi, C. Latrille, S. Esnouf, F. Bergaya, S. Le Caër, *Environmental science & technology* **2013**, *47*, 9530-9537.
[16] M. Laine, E. Balan, T. Allard, E. Paineau, P. Jeunesse, M. Mostafavi, J. L. Robert, S. Le Caer, *RSC Advances* **2017**, *7*, 526-534.
[17] M. Lainé, T. Allard, E. Balan, F. o. Martin, H. J. Von Bardeleben, J.-L. Robert, S. L. Caër, *The Journal of Physical Chemistry C* **2016**, *120*, 2087-2095.
[18] J. Ahn, R. Kopelman, P. Argyrakis, *The Journal of chemical physics* **1999**, *110*, 2116-2121.
[19] A. L. Lin, R. Kopelman, P. Argyrakis, *Physical Review E* **1997**, *56*, 6204.
[20] A. L. Lin, R. Kopelman, P. Argyrakis, *The Journal of Physical Chemistry A* **1997**, *101*, 802-808.
[21] A. L. Lin, R. Kopelman, P. Argyrakis, *Physical Review E* **1996**, *54*, R5893.
[22] M. Nakashima, E. Tachikawa, *Radiochimica Acta* **1983**, *33*, 217-222.
[23] M. Nakashima, E. Tachikawa, *Journal of Nuclear Science and Technology* **1987**, *24*, 41-46.
[24] M. Nakashima, Y. Aratono, *Radiation Physics and Chemistry* **1993**, *41*, 461-465.
[25] N. Mikio, N. M. Masaki, *Radiation Physics and Chemistry* **1996**, *47*, 241-245.
[26] H. M. Jennings, *Cement and concrete research* **2000**, *30*, 101-116.
[27] aJ. J. Thomas, H. M. Jennings, A. J. Allen, *Cement and Concrete Research* **1998**, *28*, 897-905; bH. M. Jennings, *Cement and Concrete Research* **2008**, *38*, 275-289.
[28] aJ. Bernal, J. Jeffery, H. Taylor, *Magazine of Concrete research* **1952**, *4*, 49-54; bH. Taylor, J. Howison, *Clay Minerals Bull* **1956**, *3*, 98-111; cS. Hamid, *Zeitschrift für Kristallographie-Crystalline Materials* **1981**, *154*, 189-198; dH. Kurczyk, H. Schwiete, in *Proceedings of the 4th International Symposium on the Chemistry of Cement, Vol. 1*, **1962**, pp. 349-358; eH. Stade, D. Müller, *Cement and Concrete Research* **1987**, *17*, 553-561; fK. Fujii, W. Kondo, *Journal of the American Ceramic Society* **1983**, *66*; gX. Cong, R. J. Kirkpatrick, *Advanced Cement Based Materials* **1996**, *3*, 144-156; hH. Stade, W. Wieker, *Zeitschrift für anorganische und allgemeine Chemie* **1980**, *466*, 55-70.

[29] G. Kovačević, L. Nicoleau, A. Nonat, V. Veryazov, *Zeitschrift für Physikalische Chemie* **2016**, *230*, 1411-1424.
[30] W. Wieker, A.-R. Grimmer, A. Winkler, M. Mägi, M. Tarmak, E. Lippmaa, *Cement and Concrete Research* **1982**, *12*, 333-339.
[31] S. Komarneni, D. M. Roy, C. A. Fyfe, G. Kennedy, *Cement and Concrete Research* **1987**, *17*, 891-895.
[32] C. Hoffmann, T. Armbruster, *Zeitschrift fur Kristallographie* **1997**, *212*, 864-873.
[33] S. Grangeon, F. Claret, Y. Linard, C. Chiaberge, *Acta Crystallographica Section B: Structural Science, Crystal Engineering and Materials* **2013**, *69*, 465-473.
[34] S. Le Caër, *Water* **2011**, *3*, 235-253.
[35] S. Grangeon, F. Claret, C. Lerouge, F. Warmont, T. Sato, S. Anraku, C. Numako, Y. Linard, B. Lanson, *Cement and Concrete Research* **2013**, *52*, 31-37.
[36] R. M. Barrer, *Zeolites and clay minerals as sorbents and molecular sieves*, **1978**.
[37] R. Barrer, *Pure and Applied Chemistry* **1989**, *61*, 1903-1912.
[38] C. Roosz, S. Gaboreau, S. Grangeon, D. Prêt, V. Montouillout, N. Maubec, S. Ory, P. Blanc, P. Vieillard, P. Henocq, *Langmuir* **2016**, *32*, 6794-6805.
[39] H. A. Schwarz, J. P. Losee Jr, A. O. Allen, *Journal of the American Chemical Society* **1954**, *76*, 4693-4694.
[40] H. A. Schwarz, *Journal of the American Chemical Society* **1955**, *77*, 4960-4964.